Journal of Controlled Release 362 (2023) 524–535

Contents lists available at ScienceDirect

Journal of Controlled Release

journal homepage: www.elsevier.com/locate/jconrel

Navigating chimeric antigen receptor-engineered natural killer cells as drug carriers *via* three-dimensional mapping of the tumor microenvironment

Shigao Huang [a,b,1], Fuqiang Xing [a,c,d,1], Yeneng Dai [a,c], Zhiming Zhang [a,c], Guangyu Zhou [a,c], Shuo Yang [a,c], Yu-Cheng Liu [a,c], Zhen Yuan [a,c], Kathy Qian Luo [a,c], Tianlei Ying [e], Dafeng Chu [f,**], Tzu-Ming Liu [a,c,*], Chu-Xia Deng [a,c,*], Qi Zhao [a,c,*]

[a] *Institute of Translational Medicine, Cancer Centre, Faculty of Health Sciences, University of Macau, Taipa, Macau SAR, China*
[b] *Department of Cell Biology of National Translational Science Center for Molecular Medicine and Department of Radiation Oncology of Xijing Hospital, Fourth Military Medical University, Xi' an, China*
[c] *MoE Frontiers Science Center for Precision Oncology, University of Macau, Taipa, Macau SAR, China*
[d] *Guangdong Provincial Key Laboratory of Biomedical Imaging and Guangdong Provincial Engineering Research Center of Molecular Imaging, The Fifth Affiliated Hospital, Sun Yat-Sen University, Zhuhai, China*
[e] *MOE/NHC/CAMS Key Laboratory of Medical Molecular Virology, Shanghai Institute of Infectious Disease and Biosecurity, Shanghai Engineering Research Center for Synthetic Immunology, School of Basic Medical Sciences, Fudan University, Shanghai, China*
[f] *Geneleap Biotechnology LLC, Woburn, MA, USA*

ARTICLE INFO

Keywords:
CAR-NK cells
Tumor microenvironment
Three-dimensional slice culture
Photothermal therapy
Intravital two-photon imaging

ABSTRACT

Chimeric antigen receptor (CAR)-modified natural killer (NK) cells are recognized as promising immunotherapeutic agents for cancer treatment. However, the efficacy and trafficking of CAR-NK cells in solid tumors are hindered by the complex barriers present in the tumor microenvironment (TME). We have developed a novel strategy that utilizes living CAR-NK cells as carriers to deliver anticancer drugs specifically to the tumor site. We also introduce a time-lapse method for evaluating the efficacy and tumor specificity of CAR-NK cells using a two-photon microscope in live mouse models and three-dimensional (3D) tissue slide cultures. Our results demonstrate that CAR-NK cells exhibit enhanced antitumor immunity when combined with photosensitive chemicals in both *in vitro* and *in vivo* tumor models. Additionally, we have successfully visualized the trafficking, infiltration, and accumulation of drug-loaded CAR-NK cells in deeply situated TME using non-invasive intravital two-photon microscopy. Our findings highlight that tumor infiltration of CAR-NK cells can be intravitally monitored through the two-photon microscope approach. In conclusion, our study demonstrates the successful integration of CAR-NK cells as drug carriers and paves the way for combined cellular and small-molecule therapies in cancer treatment. Furthermore, our 3D platform offers a valuable tool for assessing the behavior of CAR cells within solid tumors, facilitating the development and optimization of immunotherapeutic strategies with clinical imaging approaches.

1. Introduction

Immunotherapy has emerged as an innovative strategy for cancer treatment, with adoptive immunotherapy gaining significant attention [1]. Chimeric antigen receptor (CAR)-T cells have demonstrated remarkable efficacy in hematological malignancies and have received extensive clinical recognition [2,3]. However, owing to multifaceted factors, the biological functions of CAR-T cells are often hampered by the immunosuppressive tumor microenvironment (TME) [4–6]. Overcoming these challenges and developing effective CAR therapeutics for solid tumors has become a priority in cancer research [7,8].

Natural killer (NK) cells, offer a rapid immune response for the recognition and spontaneous elimination of tumor cells [9]. To address the immunosuppressive TME in solid tumors, the development of CAR-NK cells has gained increasing interest as a means to shape antitumor immunity [10]. CAR-NK cells offer the advantage of reduced toxicity

* Corresponding authors at: Institute of Translational Medicine, Cancer Centre, Faculty of Health Sciences, University of Macau, Taipa, Macau SAR, China.
** Corresponding author.
E-mail addresses: Dafeng.chu@luye.com (D. Chu), tmliu@um.edu.mo (T.-M. Liu), cxdeng@um.edu.mo (C.-X. Deng), qizhao@um.edu.mo (Q. Zhao).
[1] Equal contribution.

https://doi.org/10.1016/j.jconrel.2023.09.007
Received 13 April 2023; Received in revised form 31 August 2023; Accepted 3 September 2023
Available online 9 September 2023

compared to CAR-T cells, with lower risks of graft *versus* host disease (GVHD), Cytokine release syndrome (CRS), and neurotoxicity [11]. NK-92 cells, possessing phenotypic and functional characteristics similar to activated NK cells, have been extensively studied and utilized in clinical trials. These trials leverage NK-92 cell lines for their scalability in large-scale manufacturing [12]. Recent preclinical and clinical studies have extensively characterized NK-92 cells with CARs against various cancer types, including non-small cell lung cancer, leukemia, and gastric cancer [13–15]. These studies provide evidence supporting the development of CAR-NK-92 cells as a cancer therapeutic modality.

Recently, the development of diverse *in vitro* and *in vivo* methods has guided the evolution of therapeutic drugs and potential mechanistic studies of tumor immunotherapy [16,17]. Classical *in vitro* two-dimensional (2D) co-cultures have been widely used to evaluate the effector functions of immune cells. These conventional methods, which rely on the use of singularized tumor cells in a 2D monolayer culture, do not reflect the physiological properties of the TME and individual phenotypes. Although analyses of the TME can be performed using patient-derived xenograft (PDX) models, these models have low success rates and are time consuming [18]. The recent use of 3D tumor models has provided reliable tools for assessing the therapeutic efficacy of immune cells. To perform the most accurate assessment, some novel methods, including 3D tumor spheroids [19], 3D tumor slice culture (3D-TSC) [20], and tumor-derived organoids (PDOs) [21,22], have been used to recapitulate the complex tissue microenvironment *in vitro*. Preclinical studies on these organoids offer valuable pharmacodynamic indications for the therapeutic efficacy of CAR-based cells.

For adoptive immune cell therapy, antitumor efficacy is often limited by less immune cell infiltration and accumulation at tumor sites, resulting in variable responses in patients [23,24]. Although information on tumor-infiltrated immune cells can be obtained by analyzing biopsy specimens, noninvasive and dynamic assessment of response will help optimize personalized treatment regimens and combination therapies in the clinic [25]. Traditional pharmacokinetic and pharmacodynamic imaging techniques, such as magnetic resonance imaging (MRI) and positron emission tomography (PET), do not accurately reflect the trafficking, infiltration, and accumulation of immune cells in tumor sites [26,27]. These methods rely on the modification of adaptive immune cells using tracers, which can affect the biological functions of cells [28]. In addition, the spatial resolution of MRI and PET is poor for cellular-level analyses. Recently, intravital multiphoton microscopy has been employed to visualize the deep tissue dynamics of immune cells in postcapillary venules with high spatial resolution [29]. Intravital multiphoton microscopy has also been used to assess the intratumoral proliferation and intracerebral persistence of anti-CD19 CAR-T cells in solid tumor models [30]. The multiphoton imaging system is the most appropriate molecular imaging modality for validating the efficacy of CAR-NK-assisted cancer therapy.

B7-H3 is a promising target for the immunotherapy of solid tumors [31,32]. To date, both CAR-T and CAR-NK cells targeting B7-H3 have exhibited potent efficacy in preclinical and clinical studies [15,33]. In this study, we aimed to develop a drug delivery approach based on living B7-H3 CAR-NK cells engineered to direct small-molecule drugs to the tumor site (Scheme 1). Overall, the combination of immunotherapy and chemotherapeutic drug delivery can be achieved by utilizing CAR-NK cells to reduce off-target toxicity. Furthermore, a dynamic and noninvasive approach was developed to quantitatively evaluate the cytotoxic responses of CAR-NK cells in a fluorescence resonance energy transfer (FRET)-based 3D-TSC. We integrated intravital multiphoton imaging approaches for time-course visualization of the pharmacodynamics and efficacy of CAR-NK cells. This modular platform enables medical practitioners to analyze the trafficking, infiltration, and accumulation of CAR-based immune cells.

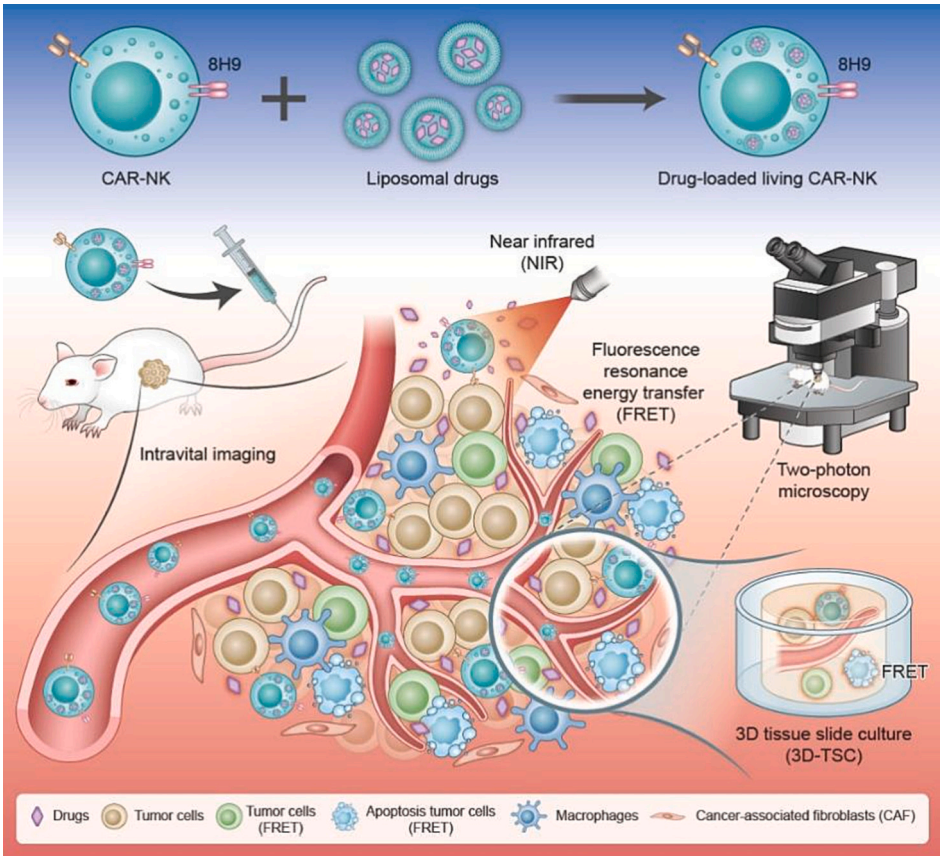

Scheme 1. Schematic illustration of intravital multiphoton imaging approaches for time-course visualization of the pharmacodynamics and efficacy of CAR-NK cells.

2. Methods

2.1. Cell lines and culture

A549 (lung carcinoma) and HeLa (cervical carcinoma) cell lines were kindly provided by the Cell Bank/Stem Cell Bank of the Chinese Academy of Sciences. A549 and HeLa cells were grown in RPMI 1640 and DMEM (Gibco) containing 10% fetal bovine serum (FBS; Gibco; Thermo Fisher Scientific Inc.), 100 U/ml penicillin, and 100 mg/ml streptomycin (Gibco). NK-92 cells were cultured in the Alpha Minimum Essential medium (GIBCO) supplemented with 0.2 mM inositol (Sigma-Aldrich), 0.1 mM 2-mercaptoethanol (Sigma-Aldrich), 0.02 mM folic acid (Sigma-Aldrich), and adjusted to achieve final concentrations of 12.5% horse serum (GIBCO), 12.5% fetal bovine serum, 100 U/ml penicillin, and 100 μg/ml streptomycin. The cells were maintained at 37 °C in a humidified incubator with 5% CO_2.

2.2. Generation of anti-B7-H3 CAR-NK cells

CAR-NK cells were generated according to the instructions previously described, with some modifications [15]. Briefly, CAR comprising the anti-B7-H3 single chain variable region (scFv), CD8 transmembrane (TM) region, and the intracellular domains of 4-1BB and CD3ζ, was cloned into the lentiviral vector carrying the reporter gene (ZsGreen or TdTomato). The lentiviral particles were produced in HEK293T cells. After NK-92 cells were transfected with the lentiviruses, CAR-expressing NK-92 cells were harvested using a FACSAria II cell sorter (BD Biosciences).

2.3. Preparation and characterization of the benzoporphyrin derivative-encapsulated liposomal nanoparticles

The liposomal benzoporphyrin derivative (LBPD) nanoparticles were produced as previously described [30]. Briefly, cholesterol (Avanti, USA), 1, 2-dipalmitoyl-sn-glycerol-3-phosphocholine (DPPC), 1, 2-distearoyl-snglycero-3-phosphoethanolamine-N-[methoxy (polyethylene glycol)-2000] (ammonium salt) (DSPE-mPEG (2000), and Benzoporphyrin Derivative (BPD) (Avanti, USA) were mixed at a molar ratio of 1:10:5:5. Thereafter, a thin lipid layer was generated using a vacuum rotary evaporator and hydrated using PBS. The liposomal structure was formed *via* six freeze–thaw cycles, and the liposome size was reduced *via* five times extrusion through a 100 nm polycarbonate membrane using an Avanti Polar Lipids syringe extruder (Alabaster, AL, USA). A UV–Vis spectrophotometer (UV-1800, Shimadzu, Japan) was used to measure the UV–Vis absorbance spectra of the prepared liposomes, and a Zetasizer NanoZS instrument (Malvern, U.K.) was used to characterize their hydrodynamic sizes (nm), polydispersity indices, and zeta potentials (mV).

2.4. Cytotoxicity assays

Tumor cell mortality was measured using a calcein-AM release assay kit (Invitrogen, US). First, CAR-NK92MI cells were incubated with liposomal BPD particles for 2 h to complete the NPs cellular uptake process. Thereafter, the CAR-NK (LBPD) cells were washed three times with PBS, resuspended in cell medium, and added to the tumor cells at a 2:1 E: T ratio; the final volume in a 96-well plate was 200 μl. The mixing cell plates were incubated at 37 °C with 5% CO_2 for 4 h. After 4 h of incubation, the laser irradiation group was irradiated with a 680 nm laser at 1 W/cm^2 for 5 min. The plate was centrifuged at 300 ×*g* for 5 min, and 100 μl of supernatant was collected from each well and transferred to a 96-well white plate. Calcein fluorescence was measured using a multimode plate reader (EnVision 2105 Multimode Plate Reader, PerkinElmer) at excitation/emission wavelengths of 495/515 nm. Tumor cell mortality was measured according to the percentage of Calcein release: % lysis = (E − S)/(M − S) × 100%, where E is the fluorescence measured in combined cultures of target and effector cells, S is the spontaneous fluorescence of the target cells, and M is the maximum fluorescence measured after lysis of all cells with buffer containing 0.5% Triton X-100, 10 mM Tris-HCl (pH 7.4), and 10 mM EDTA.

2.5. 3-dimensional tumor spheroid assays

HeLa-C3 cells were generated by incorporating a fluorescence resonance energy transfer (FRET)-based sensor to detect caspase-3 activation, as previously described [34]. Non-adhesive round-bottom 96-well plates (Sigma Aldrich, USA) were pre-coated with 1% pluronic-F127 (Sigma Aldrich) before seeding the HeLa-C3 cells. The plates were then centrifuged at 1000 ×*g* for 5 min in a Sorvall Legend XTR Centrifuge (Thermo Fisher Scientific) and incubated at 37 °C and 5% CO_2. The medium was changed every day to ensure maximal oxygen and nutrient penetration into the spheroids. Prestoblue (Invitrogen) was added to the cells each day, and the absorbance was measured 2 h after the addition of the reagents. The radii of the spheroids were measured using ten spheroid samples.

2.6. Glucose metabolism assays

The XF96 glycolysis stress test and mito stress test were performed using a Seahorse XFe96 Extracellular Flux Analyzer (Agilent) to measure the ECAR and OCR. One day prior to the assay, A549 cells were seeded at 7000 cells/well in 96-well Seahorse plates. A549 cells were treated with CAR-NK or NK cells for 24 h. The growth medium was replaced with XF assay medium and the cells were incubated in a CO_2-free incubator for 1 h. After the tests, the cells were lysed with lysis buffer (0.1% triton, 10 mM Tris–HCl), and Bradford reagent was used to determine the total amount of protein in each well. The final concentrations of the reagents used in glycolysis stress were as follows: 10 mmol/L glucose, 2 μmol/L oligomycin, and 50 mmol/L 2-deoxy-D-glucose (2-DG) in each group. The final concentrations of reagents utilized in the mito stress test were as follows: 2 μmol/L of oligomycin, 2 μmol/L of FCCP, and 0.5 μmol/L of antimycin A/rotenone in each group.

2.7. 3-dimentional tumor slice cultures (3D-TSCs) models

The 3D-TSCs (300 μm) were prepared under sterile conditions using a vibratome within 6 h after surgery according to an established protocol [20]. The slices were then carefully precoated with a collagen gel mixture (200 μL) on a 0.4-mm pore size membrane culture insert in a 24-well plate. After the tissue-containing gel was solidified, 50 μL CAR-NK cells (1,000,000) were added to the inner insert, and 450 μL of culture medium was added to the outer dish in the hood. The slice culture medium was composed of 20% fetal horse serum, 20% fetal bovine serum, and 50 μg/ml gentamicin. Later, the slices were cultivated in a humidified incubator at 5% CO_2 and 37 °C. The medium was changed every four days thereafter. The slices at different time points were removed for imaging analysis using a Leica M165FC fluorescent stereo microscope, and the MTT assay was performed to evaluate the therapeutic effect. The slices were washed three times with PBS, stained with 400 μL MTT (1 mg/mL) in 24 well plates, and incubated for 2 h at 37 °C. After incubation, the slices were washed three times with PBS, and then 800 μL of the MTT solvent (isopropanol) was added to each well. The plate was shaken on an orbital shaker for 2 h, and the absorbance was read at 570 nm using a plate reader (Perkin Elmer Victor X3, Waltham, MA, USA). All present tumor slices were fixed with 10% formalin and embedded in paraffin for immunohistochemistry (IHC) stain. The IHC toolbox ImageJ software was used to analyzed proportion of the brown color of H-DAB stained images.

2.8. In vivo therapy of CAR-NK cells

NOD/SCID mice (male, aged 4–6 weeks) were subcutaneously administered 1.7×10^6 A549 cells with more targeting ability. Animals were randomized into the seven treatment groups ($N = 6$ per group). Mice were intravenously administered PBS, LBPD, CAR-NK(LBPD), and CAR-NK cells on days 14, 21, and 28, respectively. The tumor size and weight were recorded every 5 days, and tumor volume was calculated according to the following formula: volume $= 0.5 \times \text{width}^2 \times \text{length}$. The survival time was recorded, and dead mice were stored for further use. All experimental animal protocols were approved by the Ethics Committee of the University of Macau Animal Faculty (UMARE – 041–2020).

2.9. Intravital multiphoton microscopy

A real-time multiphoton-photon microscopy system (Fig. S5A) was used to image and observe NK cell distribution *in vivo*. A Nikon A1MP+ fluorescence confocal microscope (Nikon, Japan) was used with a water-immersed 40× (NA = 1.15) objective. Two-photon laser excitation was performed using an 800–1300 nm tunable femtosecond laser (Insight X3, Spectra Physics). Before observation, mice were anesthetized *via* an intraperitoneal injection of Avertin (25 μL injection volume per gram of body weight). Thereafter, mice were mounted on a 2 cm bottom glass Petri dish and the tumor was exposed for observation. Intravenous catheters were used to inject the cells (CAR-NK(LBPD) cells in 100 μL PBS) *via* the tail vein. Intravital multiphoton images of the tumor microenvironment were acquired using near-infrared 1300 nm excitation. The third harmonic generation (THG) signals of blood cells [35], two-photon fluorescence (TPF) of CAR-NK(LBPD) cells, and second harmonic generation (SHG) signals of collagens in the tumors of nude mice were collected in the wavelength ranges of 415–485 nm, 506–593 nm, 604–679 nm, and 698–750 nm, respectively.

To outline the distribution of blood vessels in the tumor microenvironment, we performed two-photon angiography with 2 megadalton dextran-FITC (Movie S3). The fluorescence (λ_{em} = 506–593 nm) of circulating dextran-FITC *in vivo* was imaged at an excitation wavelength of 970 nm.

2.10. Statistical analyses

All data are expressed as mean ± SEM. Statistical analysis was conducted using analysis of variance, Student's *t*-test, and Kaplan-Meier survival analysis. All analyses were performed using GraphPad Prism software version 8 (GraphPad Software, Inc., CA, USA). *P* values are presented as * $p < 0.05$, ** $p < 0.01$, *** $p < 0.001$, and **** $p < 0.0001$.

3. Results

3.1. Significant uptake of nanoparticles in CAR-NK cells

We aimed to develop a drug delivery system based on living NK92 cells to express anti-B7-H3 CAR. This delivery system consisted of a single-chain variable fragment (scFv) of anti-B7-H3 antibody, CD8 transmembrane domain, and intracellular 4-1BB and CD3ζ signaling domains. Human CAR-NK cells were generated *via* transduction with lentiviral constructs containing either Zs-Green or Td-Tomato reporters. CAR-NK cells were enriched using fluorescence-activated cell sorting (FACS). Flow cytometry analysis confirmed the successful expression of CAR molecules based on the detection of fluorescent Zs-Green and Td-Tomato reporters (Fig. S1). The two fluorescent formants of CAR NK cells displayed high viability (> 99%).

Liposomal nanoparticles (NP) encapsulating therapeutic agents have shown pharmaceutical value as drug delivery vehicles. Here, we prepared a biocompatible and nontoxic liposomal NP (LBPD; size, 156 nm and potential, −11.8 mV) by formulating a benzoporphyrin derivative (BPD) into liposomes, as illustrated in Fig. 1. BPDs, as photosensitizers, display photodynamic and photothermal efficacy [36,37]. To reduce the toxic effects on the cell carriers, we encapsulated them into liposomes (LBPD) with a hydrodynamic diameter and a zeta-potential of −11.8 mV (Fig. 1A). Thereafter, we loaded LBPD into living CAR-NK92 cells, achieving stable labeling (Fig. 1B). Cell viability was maintained in CAR-NK cells loaded with LBPD. Confocal fluorescence imaging confirmed the effective co-localization of LBPD fluorescence (red) with CAR NK cells (green). The optimal incubation time for better LBPD loading efficiency was approximately 2 h (Fig. 1C and Fig. S2A, B). After incubation with CAR-NK92 cells, 20 mM LBPD achieved the strongest fluorescence signals (Fig. 1D and Fig. S2C). The time-dose LBPD fluorescence curve revealed that the internalization of LBPD into CAR-NK cells reached a maximum of 25% after 2 h of incubation (Fig. 1E). The effect of LBPD on NK cell viability was determined using the Cell Counting Kit-8 (CCK-8) method on different days. The percentage of cell viability was not significantly different between the drug-loaded CAR NK cells and CAR NK cells (Fig. 1F).

3.2. Enhanced cytotoxicity ability of CAR-NK cells carrying LBPD

To determine whether NK cell function remained under drug-loading conditions, we evaluated the cytotoxic efficacy of LBPD-loaded CAR-NK cells (CAR-NK-LBPD) by co-culturing CAR-NK cells with B7-H3-positive HeLa cells as targets. Without laser irradiation, CAR-NK-LBPD led to a mortality similar to CAR-NK (approximately 30%). This finding implies that LBPD loading did not affect the cytotoxic capabilities of CAR NK cells. After illuminating the CAR-NK-LBPD cells with NIR laser light (680 nm), LBPD-mediated photothermal effects on the target cells were observed. Compared with the CAR-NK-LBBP group with laser irradiation, laser irradiation significantly increased cell mortality from 30 to 90% (Fig. 1G).

3.3. Quantitative analysis of CAR-NK-mediated cytotoxicity in FRET-based 3D-TSCs models

To determine the apoptotic effects of CAR-NK cells on cancer cells, we introduced a caspase-3 responsive fluorescence resonance energy transfer (FRET) biosensor in four cancer cell lines to generate the sensor cells, Hela-C3, MDA-MB-231, PANC1-C3, and A549-C3 [38]. The FRET reporter is a pair of cyan fluorescent protein (CFP) and yellow fluorescent protein (YFP). The FRET energy effect indicates the occurrence of apoptosis. When apoptosis is induced by NK cells, the DEVD linker of the reporter is cleaved by caspase 3 proteases, and the emission energy of CFP is transferred to YFP. Apoptotic cancer cells appear blue. This FRET detection allows real-time tracking of the apoptosis of living cells.

To validate the apoptotic effects of drug-loaded CAR-NK cells, we first established a 3D sphere model by coculturing Hela-C3 cells and LBPD-loaded CAR NK cells. During the co-culture process, the apoptotic status of cancer cells at different E: T ratios (0.5, 1, and 2) was observed. Therefore, we confirmed that Hela-C3 apoptosis was induced by the administration of CAR NK cells at different E: T ratios (Fig. S3).

To mimic the *in vivo* tumor microenvironment, 3D-TSCs were used as reliable models for the quantitative measurement of anticancer drug sensitivity [20]. Here, as shown in Fig. 2, we further established a FRET-based time-lapse and MTT endpoint assay to predict the efficacy of CAR-NK cells in 3D-TSCs. Briefly, four cancer cell lines, MDA-MB-231-C3, A549-C3, HepG2-C3, and PANC-1-C3, were subcutaneously injected into nude mice. Histological analysis of 3D-TSCs indicated B7-H3 expression (Fig. S4). Tumor tissue derived from nude mice was embedded with agarose and sectioned using a vibrating microtome. The slices were then embedded in a collagen gel on membrane inserts, and microscopic imaging of the therapeutic response was performed. After treatment of the sensor-assembled tissues with CAR-NK cells, the response of 3D-TSCs to CAR-NK cells *ex vivo* was determined by the FRET ratio in a dose- and time-dependent manner. The MTT assay of cell

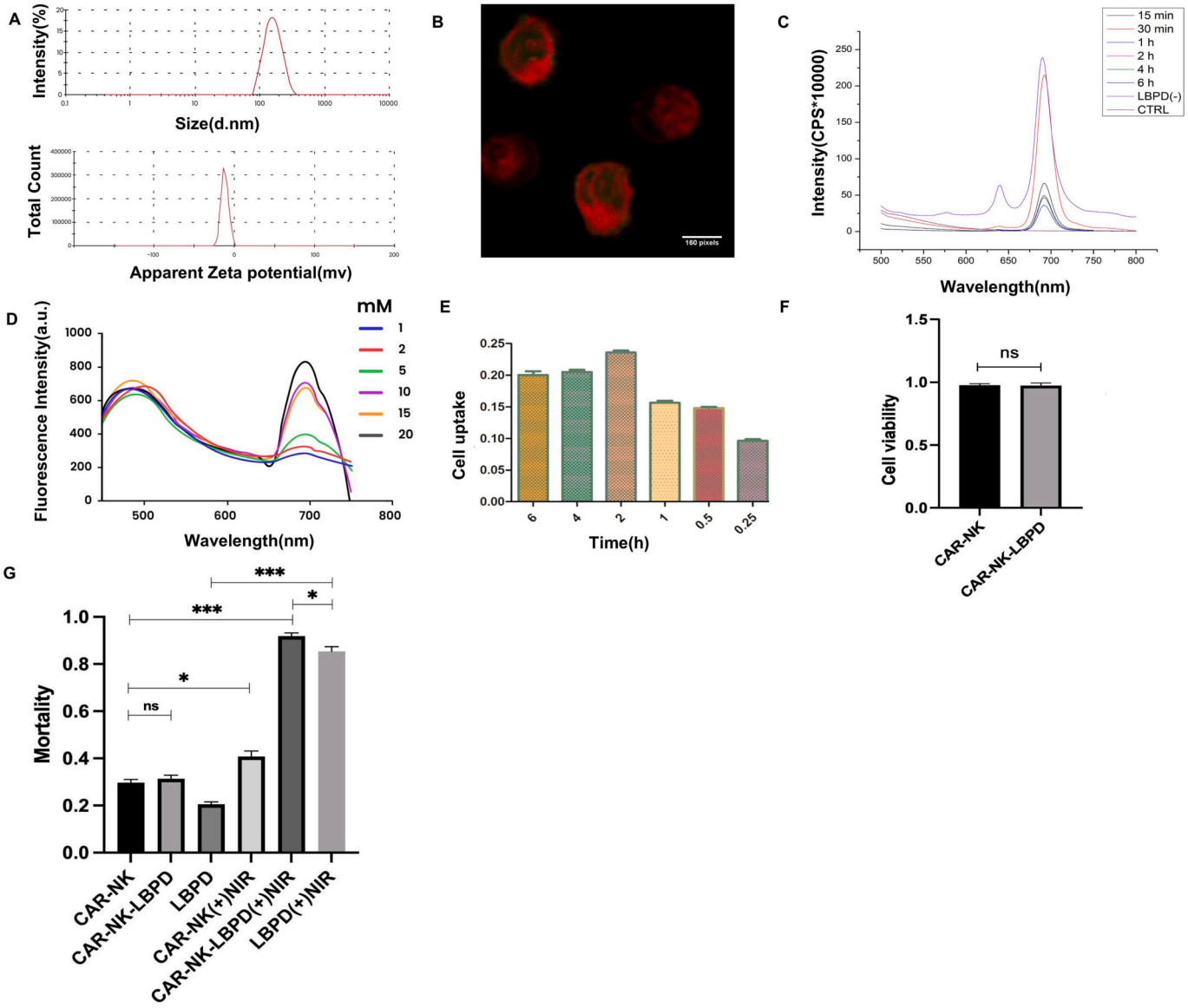

Fig. 1. Preparation and tumor cytotoxicity of LBPD-loaded CAR-NK cells. (A) Hydrodynamic size and zeta potential of LBPD liposomes were evaluated by dynamic light scattering (DLS) measurement. (B) The image of CAR-NK cell internalized LBPD by a two-photon microscope (Scare bar = 160 pix). (C—D) The fluorescence spectra of LBPD-loaded CAR-NK cells at different incubation times (C) and incubation concentrations (D). (E) The cell uptake of LBPD NPs in CAR-NK cells at different incubation times. (F) MTT showed no significant difference in the cell viability of the unlabeled or labeled CAR-NK cells. (G) Mortality of A549 cells under different treatment conditions. Data are expressed as Mean ± SEM. $^{*}p < 0.05$; $^{***}p < 0.001$.

viability was quantitatively measured.

3D-TSCs derived from MDA-MB-231-C3 cells were treated with increasing doses of CAR NK cells for seven days. The FRET ratio significantly decreased after the administration of high doses of CAR NK cells (10^6/ml and 10^7/ml) (Fig. 3A, B). Cell viability was quantified using an MTT assay. Similar to the reduced FRET ratios, the number of cells markedly decreased after CAR-NK cell treatment (Fig. 3B). To further examine repeatability and operability, we evaluated four different types of cancer cells, MDA-MB-231-C3, A549-C3, HepG2-C3, and PANC-1-C3 (Fig. 3C). Compared to untreated controls, 3D-TSCs displayed high sensitivity to CAR NK cells. The FRET and MTT assays confirmed the increase in tumor apoptosis and decrease in tumor cell numbers induced by CAR-NK cells (Fig. 3D, E). These data illustrate that 3D-TSCs could serve as valuable tools for time-lapse evaluation of CAR-engineered NK cells.

3.4. CAR-NK cells exhibit biocompatibility and low organ toxicity as drug carriers

We attempted to confirm whether the photothermal property of LBPD was retained in CAR-NK cells with LBPD loading. The temperature of the LBPD in CAR-NK cells markedly increased under laser irradiation, whereas no obvious temperature elevation of either unloaded CAR-NK cells or PBS was observed (Fig. 4A, B). Drug-loaded CAR-NK cells displayed excellent concentration- and laser power density-dependent photothermal properties under laser irradiation.

High accumulation of drugs in tumors is a prerequisite for achieving enhanced antitumor therapeutic outcomes. To compare the tumor association of CAR-NK cells to liposomes *in vivo*, we injected CAR-NK (LBPD) and LBPD with equal concentration of LBPD from tail vein. The association of BPD in tumor tissues was imaged at 12 h post injection (Fig. 4C). The results suggest that CAR-NK (LBPD) group demonstrates superior tumor accumulation and retention compared to LBPD.

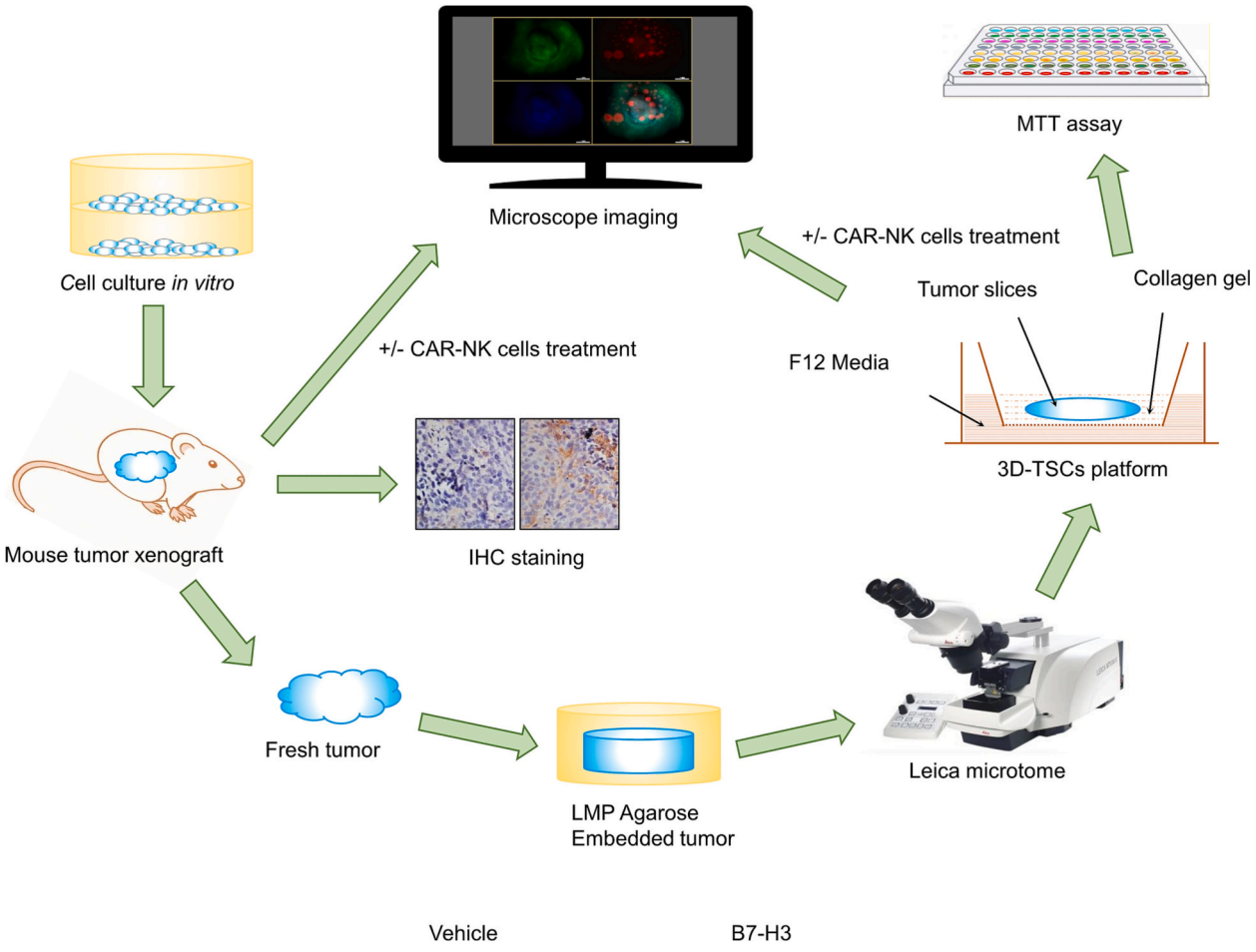

Fig. 2. A FRET-based time-lapse and MTT endpoint assay of CAR-NK cells in 3D-TSCs. Cancer cell lines MDA-MB-231-C3, A549-C3, HepG2-C3, and PANC-1-C3 are established by transfection of Sensor C3 plasmid into cells followed by subcutaneous injection of nude mouse. Tumor tissue derived from nude mouse are embedded with agarose and sectioned at a thickness of 300 μm with a vibrating microtome. The slices are then carefully embedded by collagen gel on membrane inserts in 24-well plates for slice culture and microscope imaging of therapeutic response.

To visualize LBPD biodistribution *in vivo*, the major organs were excised and the fluorescence intensities of BPD were measured in major organs (heart, liver, spleen, lung, and kidney) (Fig. 4D). BPD residue was relatively low in the heart, spleen, and lungs of the two groups. Free LBPD mice displayed high fluorescence intensity of BPD in the liver because the liver is the main organ of metabolism. In contrast, less BPD retention was observed in the liver of CAR-NK-LBPD mice.

3.5. Synergistic therapy of CAR-NK cells carrying LBPD in vivo

To evaluate the antitumor efficacy of CAR NK cells carrying drugs *in vivo*, A549 tumor-xenografted mice were intravenously administered three injections of free LBPD, CAR-NK, and CAR-NK(L-BPD) on days 14, 21, and 28, respectively (Fig. 5A). After 24 h, the tumor location was exposed to 680 nm laser irradiation for 30 s, and the tumor size was monitored by caliper measurement seven days post-tumor inoculation. Compared to the placebo group, tumor growth was inhibited in all treatment groups (Fig. 5B). According to the volume changes of the tumor, the groups treated with CAR-NK (LBPD) plus laser irradiation displayed significantly enhanced tumor cell eradication compared with the groups without laser irradiation. Combination treatment with CAR-NK cells and photothermal therapy did not affect mouse weights over the entire experimental period. Meanwhile, the overall survival of mice was significantly prolonged and even reached five months, indicating that mice could tolerate CAR-NK-mediated drug delivery (Fig. 5C). These results indicate that CAR-NK(LPBD)-mediated therapy effectively inhibited tumor growth and prolonged mouse survival through synergistic immunotherapy.

3.6. Tumor infiltration of CAR-NK cells based on intravital two-photon imaging

Based on the *in vivo* therapeutic efficacy, we opted to validate whether CAR NK cells effectively delivered drugs to tumor sites. A multiphoton microscopy system was used to confirm the targeting of CAR NK cells to tumor sites *in vivo* (Fig. S5). Prior to intravenous administration, the multiphoton contrast of CAR-NK-LBPD cells *in vitro* was examined. Red fluorescence of LBPD internalized in green CAR NK cells was observed (Fig. 6A; Movie S1 of Supporting Information). Following the treatment process (Fig. 6B), we monitored the tumor microenvironment *in vivo*. First, the third-harmonic generation (THG) contrast (magenta in Fig. 6C) was used to identify the vessels in the tumor microenvironment [35]. Thereafter, the previously infiltrated CAR-NK cells (cyan color) containing BPD (red color) were identified in the extravascular collagen networks (green color in merged images) (Fig. 6C, Fig. S6, Movie S2), where NK cells can enter tumor sites. After another injection of the cells, the fluorescent signals of infiltrated CAR-NK cells were observed by two-photon images (Fig. 7A, B). The fluorescence intensity of CAR-NK cells was found to gradually increase in a time-dependent manner by analyzing tumor-infiltrated immune cells with flow cytometry and tumor slices (Fig. 7C, D). Of note, we did not observe similar infiltration patterns, with barely any LBPD-NPs or

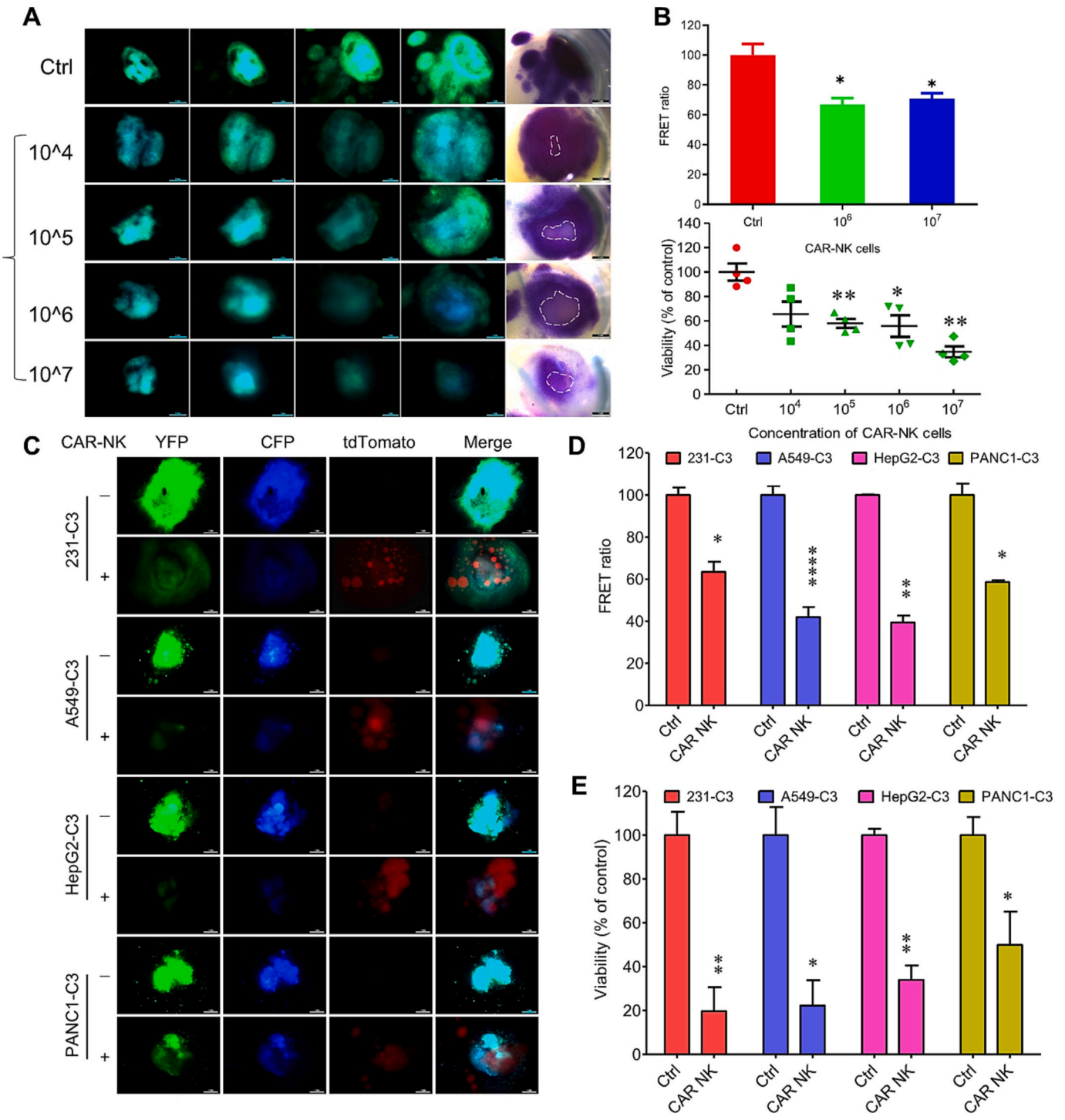

Fig. 3. Tumor-apoptosis assay of CAR-NK (red) in 3D-TSCs. (A) Merged YFP (green)/CFP (blue) images and MTT assay images of Hela-C3 cells treated with different concentrations (10^4, 10^5, 10^6, and 10^7 cells/ml) of CAR-NK cells. Scale bar, 200 μm. (B) Corresponding FRET ratios and cells viabilities in (A). The FRET ratio is estimated from the relative CFP intensity, and the cell viability is evaluated from the absorption of MTT-assay images. (C-E) Treatment responses of mouse 3D-TSCs to B7-H3 CAR-NK cell therapy at day 7 after treatment. (C) The YFP (green), CFP (blue), td-Tomato labeled NK cells (red), and merged images of various cell lines (231, A549, HepG2, and PANC1) with or without CAR-NK cell treatment. Scale bars: 200 μm. (D) FRET ratios and (E) cell viabilities of (C) with 4 technical replicas. Data are expressed as Mean ± SEM. $^*p < 0.05$; $^{**}p < 0.01$. $^{****}p < 0.0001$. The graphs are representative of the results obtained in this experiment, repeated three times. (For interpretation of the references to color in this figure legend, the reader is referred to the web version of this article.)

dextran (Movie S3). Overall, the LBPD-loaded CAR-NK cells could cross the barrier of the vessels and reach the tumor site *via* tail vein injection.

4. Discussion

Cellular immunotherapy has led to remarkable advances in preclinical and clinical applications. Live immune cells have emerged as smart carriers for delivering anticancer drugs deep within the tumor

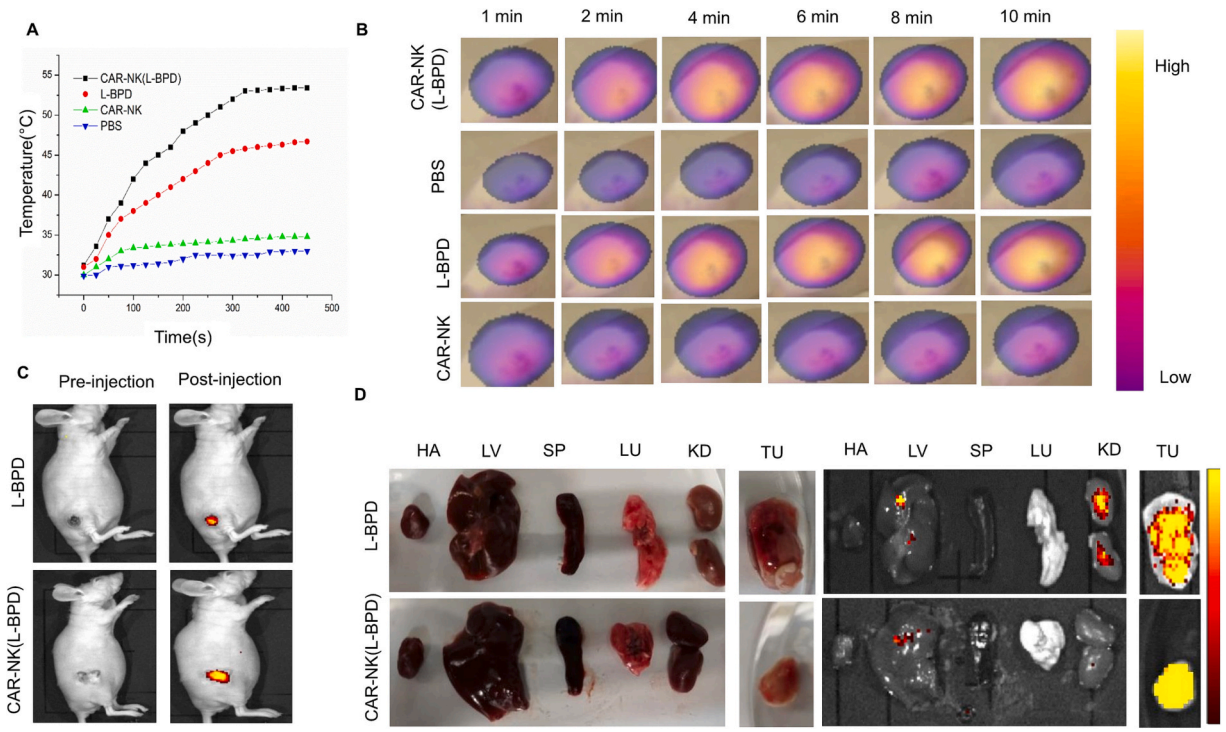

Fig. 4. *In vivo* photothermal therapeutic effect and biodistribution of drug-loaded CAR-NK cells. (A) Quantitative analysis of temperature changes in the tumor area at different time points. (B) Thermal images of A549 tumor-bearing mice treated with PBS, liposome BPD, CAR-NK, and CAR-NK(L-BPD); Cell dose was 5.2×10^6 cells and LBPD dose was 5.8 mg/kg (i.v. 100 μL) with 680 nm laser illumination at indicated time points. The laser power density was 1.0 and 1.4 W/cm^2. (C) Tumor association with BPD fluorescence of CAR-NK(L-BPD) and L-BPD groups with i.v. injection into A549 tumor-bearing mice. (D) All kinds of organs and tumor tissue are distributed significant differences with BPD fluorescence between CAR-NK(L-BPD) and L-BPD groups. (HA, LV, SP, LU, KD and TU represent heart, liver, spleen, lung, kidney and tumor).

microenvironment [39]. These live engineered cells may survive and traffic to intratumoral sites while maintaining their antitumor effector activities. Such synergistic strategy not only reduces the *in vivo* toxicity of drugs but also enhances effective drug accumulation at tumor sites. Drug-loaded live immune cells have the unique merits of natural cell functions to participate in immune regulation. CAR-engineered NK cells have shown significant promise as an "off-the-shelf" vehicle for targeted drug delivery to the tumor site. In the present study, we developed a TME-directed drug delivery vehicle using intracellular drug loading in live CAR-NK cells. As liposomes possess excellent biodegradability and biocompatibility, they are ideal drug carriers. BPD can be loaded into CAR-NK cells with the fusion of liposomes, exhibiting excellent compatibility and low cytotoxicity [40]. The therapeutic efficacy of CAR NK cells was successfully increased *in vivo* and *in vitro*.

Photothermal therapy is considered one of the most effective phototherapies that causes cancer cell death to achieve antitumor effector functions. One of the attractive features of photothermal therapy is the commonly used light-absorbing photothermal agent with activation properties that utilize non-ionizing radiation, such as near-infrared laser light [41,42]. The light-active cell drug system provides a novel option for controlled release compared with conventional liposome systems [43]. Recently, numerous synergistic therapeutic approaches have been developed for oncology. However, PDT has certain limitations when it comes to depth penetration, making it less effective for treating certain types of cancer or conditions located deep within the body. It is primarily used for superficial conditions like certain skin cancers, including melanoma. It's important to consider the limitations of PDT, including depth penetration, when discussing its clinical applicability. In this study, we investigated the localization and therapeutic potential of CAR-NK cells loaded with small molecule drugs in a subcutaneous tumor model in mice. To track the distribution of the loaded drugs, we employed a photosensitizer as an indicator. Initially, NK cells, engineered with an anti-B7-H3 CAR, recognized A549 cancer cells, initiating the targeting process. Subsequently, upon irradiation with a 680 nm laser, the photosensitized drugs were released from the CAR-NK cells. The released drugs exhibited an ablative effect on the tumor cells, highlighting the effective delivery of small molecule drugs to the tumor sites by CAR-NK cells. By utilizing a photosensitizer-based tracking system, we successfully visualized the distribution of these drugs within the subcutaneous tumor in a mouse model.

The TME cannot be clearly observed using a single-photon confocal microscope. Further, two photons can penetrate deeper than the visible wavelengths used in a confocal microscope. Our study revealed how the *in vivo* pharmacodynamics of cellular drugs can be evaluated in the TME. We employed a near-infrared laser-excited multiphoton imaging system to visualize the delivery process in deep tissues and confirmed that infiltrating CAR-NK cells could effectively transport drugs into the tumor tissue. In addition, intravital multiphoton imaging was employed to address the CAR-NK cell infiltration-mediated delivery of photosensitized drugs in the tumor. Using a tumor xenograft model, we explored the molecular mechanism of CAR-NK cell infiltration for the transport of photosensitized drugs using an intravital microscope. Tumor infiltration by CAR-NK cells led to the effective transport of drugs into the tumor tissue. The Warburg effect is a feature of metabolic dysregulation that occurs during malignant transformation. Herein, drug-loaded CAR-NK cells decreased the basal extracellular acidification rate (ECAR) and increased the basal oxygen consumption rate (OCR) (Fig. S7), serving as indicators of the anti-Warburg effect. Therefore, in addition to their apoptosis and photothermal abilities, drug-loaded CAR-NK cells may regulate glucose metabolism in cancer cells.

Significant efforts are being dedicated to preclinical studies that aim to evaluate the antitumor function of adoptive immunotherapy to provide clinical proof of concept [44–46]. In the majority of clinical trials, NK cell doses typically range between 5×10^6 and 5×10^7/kg [47]. A

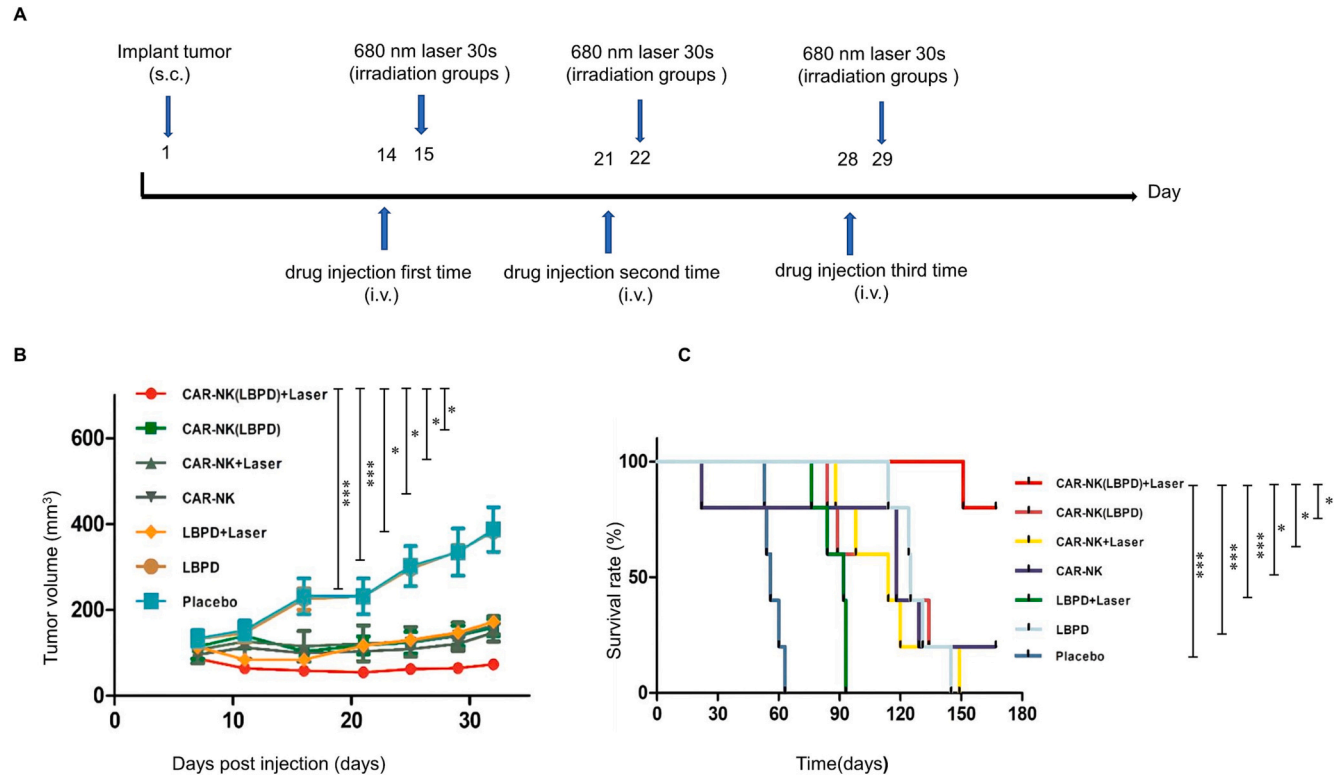

Fig. 5. *In vivo* synergistic therapy of CAR-NK cells carrying drugs. (A) Schematic diagram of the treatment regimen for validating the therapy efficiency of CAR-NK (LBPD). Mice were subcutaneously injected with 1.7×10^6 A549 cells and were divided into seven treatment groups. Mice were intravenously administered LBPD, PBS, CAR-NK(LBPD), and CAR-NK cells on day 14, day 21, and day 28. The cell dose was 5.2×10^6 cells (i.v. 100 μL) and the LBPD dose was 5.8 mg/kg for LBPD NPs, the second day every time irradiation with 680 nm laser. (B—C) Therapy of CAR-NK cells carrying drugs in tumor xenografts. Tumor size (B), and survival rate (C) of the mice bearing tumor after the injection of LBPD, CAR-NK, and CAR-NK(LBPD) were analyzed, respectively. For the placebo group, only PBS (pH 7.4) was injected without irradiation. Data are represented mean ± standard deviation ($n = 6$ mice per group) ($^*p < 0.05$, $^{***}p < 0.001$). The p values of tumor volume and survival curves among the different groups was assessed by the Kaplan-Meier analysis.

recent study demonstrated the safe administration of a dose of 1×10^8/kg CAR-NK92 cells per patient [48]. In this study, despite using a dose of approximately 1×10^8 /kg CAR-NK92 cells to treat mice, no significant adverse effects were observed. Before conducting the clinical trial for anti-B7-H3 CAR-NK92, we will explore further optimization of safety dosages.

However, the conventional 2D analysis models used in most preclinical studies do not adequately reflect the physiology of native tumors, which serves as a limitation [20]. While PDX models offer significant advantages, their high costs and low success rates present challenges in preclinical and clinical applications. However, our study introduces a pioneering approach where we utilize the 3D-TSC (Three-Dimensional Tumor Spheroid Culture) as an *ex vivo* model to investigate the effects of CAR-NK therapy. This is the first report of utilizing the 3D-TSC model for such purposes. Our study presents a method for quantitatively analyzing the cytotoxic activity of CAR-NK cells within the 3D-TSC model. The C3-mediated 3D-TSC model was employed to evaluate the effectiveness of CAR-NK cells. Our findings demonstrate that CAR-NK cells exhibit efficient cytotoxicity specifically targeted towards tumor organoids within the 3D-TSC model. These results hold promising implications for the development of a rapid and individualized protocol for utilizing CAR-NK cells in preclinical studies. The discovery of CAR-NK cells' effective targeting of tumor organoids within the 3D-TSC model provides valuable insights. This finding has the potential to advance the development of more efficient and personalized approaches to CAR-NK cell therapy in preclinical settings. It paves the way for the exploration of rapid and individualized protocols, contributing to the advancement of CAR-NK cell research and their potential translation into clinical applications.

5. Conclusion

In summary, we established a new cellular therapeutic drug delivery system that integrates CAR NK cell immunotherapy with light activation of small-molecule prodrugs. Drug-loaded living NK cells exhibit enhanced antitumor activity *in vitro* and *in vivo*. More importantly, by integrating 3D-TSCs with intravital multiphoton imaging techniques, we have developed a cutting-edge approach for the rapid assessment of the apoptosis effects of CAR-NK cell therapy. This innovative strategy allows for real-time 3D evaluation of CAR-NK cell therapy efficacy *in vivo* or human tumor tissue using a two-photon microscope, eliminating the need to wait for complete tumor extinction. Consequently, this method enables clinics to select the most appropriate CAR-NK drugs from the outset, improving treatment decision-making and optimizing patient outcomes.

Supplementary data to this article can be found online at https://doi.org/10.1016/j.jconrel.2023.09.007.

Ethical approval and consent to participate

All experimental animal protocols were approved by the Ethics Committee of the University of Macau Animal Faculty (UMARE – 041–2020).

Consent for publication

Not applicable.

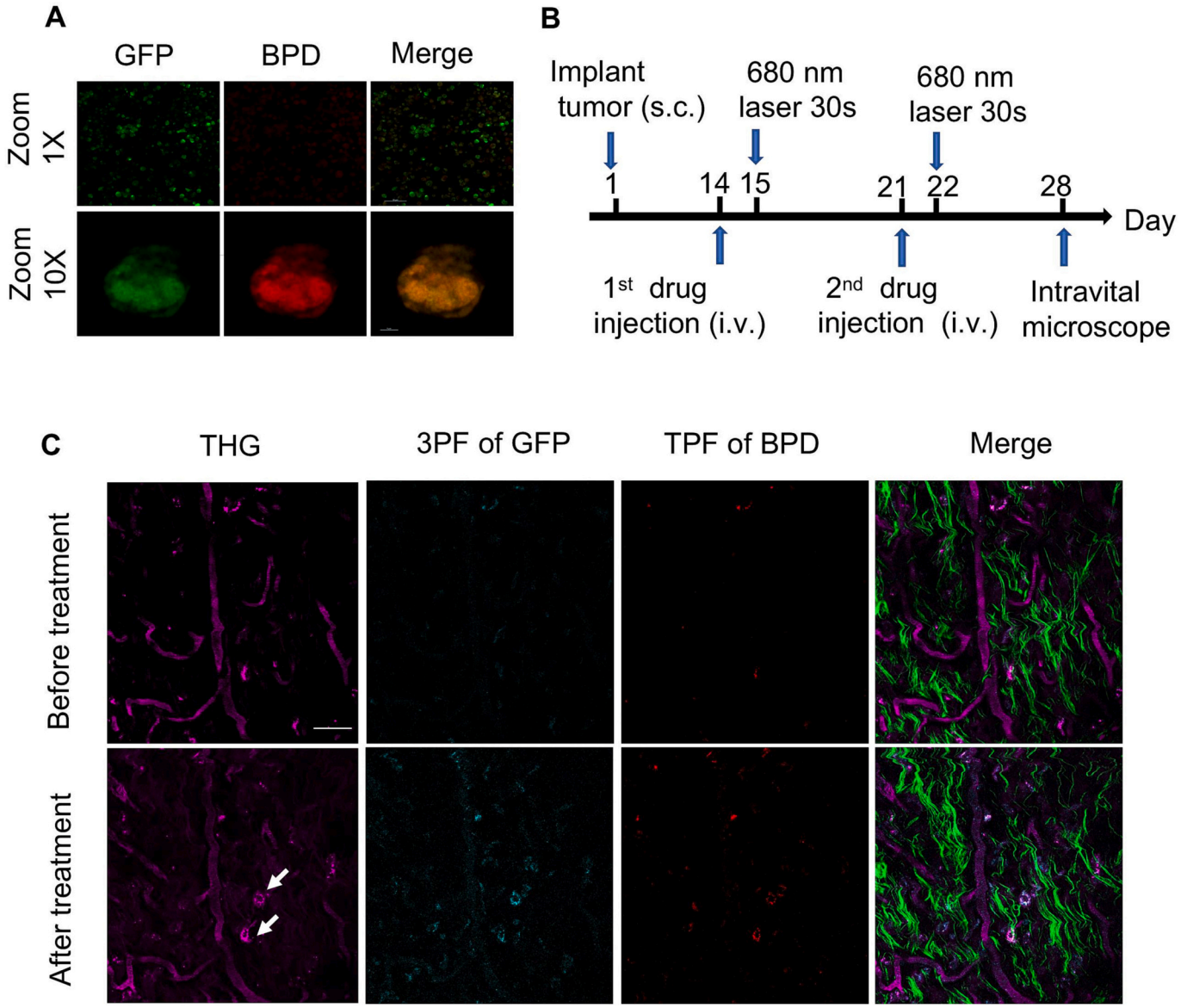

Fig. 6. CAR-NK cell delivery of BPD across the blood vessel barrier into the tumor tissues after priming photosensitization. (A) Two-photon fluorescence image of transgenic-labeled NK cells (green) and modifications of LBPD NPS fluorescence (red), view in Zoom x10 magnification time CAR-NK cell around with LBPD NPs, Scale bars, 50 μm. (See movies S2 and S3 for more details). (B) The process of intravital microscopic from CAR-NK(LBPD) injection and treatment to tumor tissues. (C) Intravital microscopic images of a mouse treated by CAR-NK(LBPD) (pink in merge photograph). The experimental protocol of intravital microscopy of tumors is illustrated in the method. When the CAR-NK (LBPD) was i.v. administrated. CAR-NK (LBPD) (pink) was across and around the tumor vessel (blue) and SHG collagen (silvery grey) Scale bars, 50 μm. (For interpretation of the references to color in this figure legend, the reader is referred to the web version of this article.)

Funding

The study is supported by the National Key Research and Development Program of China (2019YFA0904400), the Science and Technology Development Fund, Macau SAR (File no. FDCT/0043/2021/A1, FDCT 0120/2020/A3 and FDCT/0002/2021/AKP), the Multi-Year Research Grant of the University of Macau (MYRG-CRG2022-00009-FHS, MYRG-GRG2023-00053-FHS-UMDF, MYRG2022–00143-FHS and MYRG-GRG2023-00158-FHS-UMDF), the Natural Science Foundation of Guangdong Province (2023A1515010549), Shenzhen Science and Technology Project (SGDX2020110309280301, EF040/FHS-DCX/2021/SZSTIC), Dr. Stanley Ho Medical Development Foundation (SHMDF-VSEP/2022/002), and Zhong Nanshan Medical Foundation of Guangdong Province (ZNSA-2021016).

CRediT authorship contribution statement

Shigao Huang: Writing – review & editing, Writing – original draft, Validation, Methodology, Investigation, Formal analysis, Data curation, Conceptualization. **Fuqiang Xing:** Validation, Investigation, Data curation. **Yeneng Dai:** Investigation, Data curation. **Zhiming Zhang:** Validation, Formal analysis. **Guangyu Zhou:** Validation, Investigation. **Shuo Yang:** Validation, Formal analysis. **Yu-Cheng Liu:** Visualization, Formal analysis. **Zhen Yuan:** Formal analysis, Data curation. **Kathy Qian Luo:** Methodology, Formal analysis. **Tianlei Ying:** Methodology, Formal analysis. **Dafeng Chu:** Supervision, Project administration, Conceptualization. **Tzu-Ming Liu:** Writing – review & editing, Supervision, Project administration, Methodology. **Chu-Xia Deng:** Supervision, Resources, Project administration, Methodology. **Qi Zhao:** Writing – review & editing, Resources, Project administration, Funding acquisition, Conceptualization.

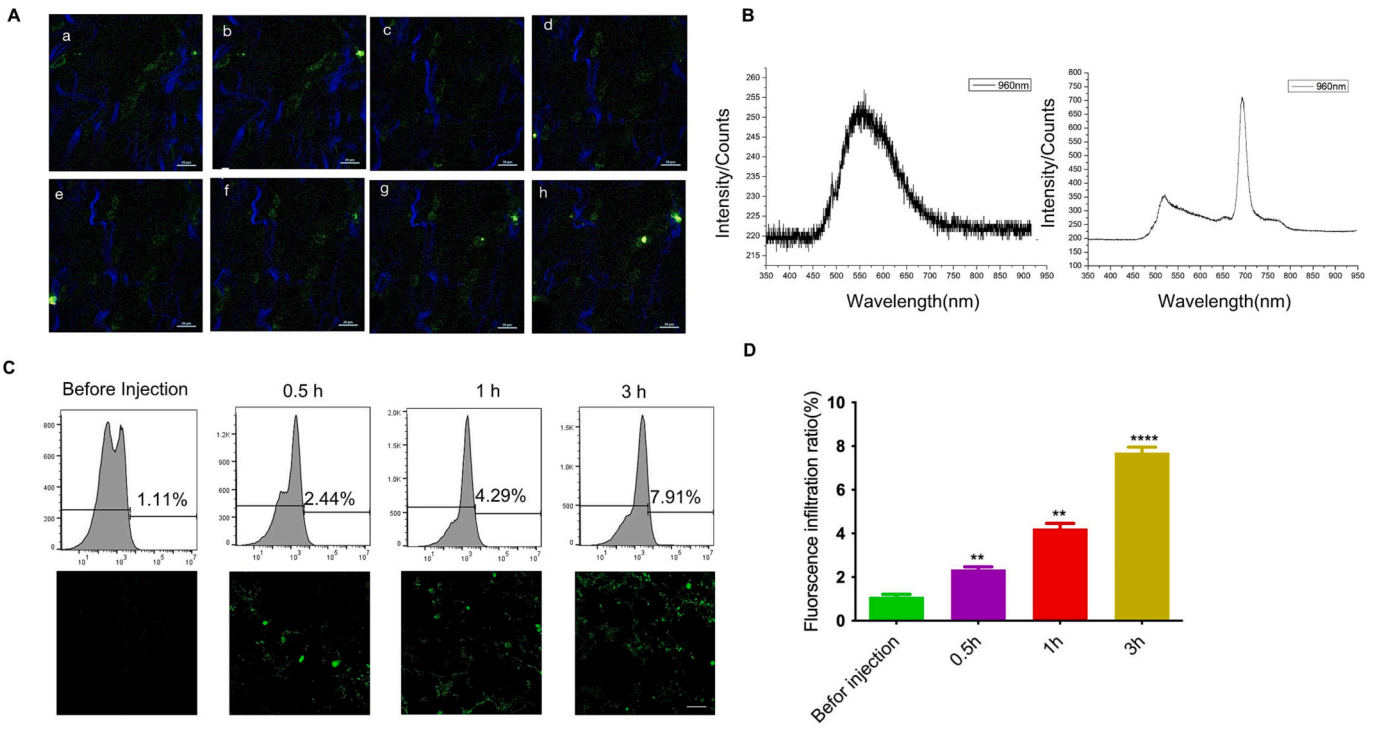

Fig. 7. CAR-NK cell infiltration dynamics in the local tumor area (A) The 960 nm excited two-photon images of infiltrated CAR-NK cells (green color) at different regions(a-h) of tumor tissues *in vivo*. Blue color represents the extravascular collagen networks. Scale bars: 50 μm (B) The 960-nm excited two-photon fluorespectra of CAR-NK (top) and CAR-NK-LBPD cells (down). In CAR-NK cells without labeling, we could only observe weak flavin fluorescence peaked around 550 nm. For CAR-NK-LBPD cells, we observed 520 nm peak of ZsGreen and 690 nm peak of BPD, respectively. (C) The fluoresce intensity and images of CAR-NK cells infiltration dynamics before and at the 0.5, 1, 3 h post injection by flow cytometer analysis and tumor slices. Scale bars: 20 μm. (D) The quantitative results of the increase of CAR-NK-cell infiltration in the local tumor area with flow cytometry at the 0.5, 1, 3-min post injection. Data are expressed as Mean ± SEM. $^{**}p < 0.01$. $^{****}p < 0.0001$. The graphs are representative of the results obtained in this experiment, repeated three times. (For interpretation of the references to color in this figure legend, the reader is referred to the web version of this article.)

Declaration of Competing Interest

The authors declare no conflict of interest.

Data availability

All data generated or analyzed during this study are included in this published article and its supplementary information files.

Acknowledgments

We thank the anti-B7-H3 antibody 8H9 from Dr. Nai-Kong V. Cheung (MSKCC). We appreciate supporting of Animal Facility, University of Macau.

References

[1] Y. Peng, S. Fu, Q. Zhao, 2022 update on the scientific premise and clinical trials for IL-15 agonists as cancer immunotherapy, J. Leukoc. Biol. 112 (2022) 823–834.
[2] S. Grupp, M. Kalos, D. Barrett, R. Aplenc, D. Porter, S. Rheingold, D. Teachey, A. Chew, B. Hauck, J. Wright, M. Milone, B. Levine, C. June, Chimeric antigen receptor-modified T cells for acute lymphoid leukemia, N. Engl. J. Med. 368 (2013) 1509–1518.
[3] Q. Zhao, M. Ahmed, D.V. Tassev, A. Hasan, T.Y. Kuo, H.F. Guo, R.J. O'Reilly, N. K. Cheung, Affinity maturation of T-cell receptor-like antibodies for Wilms tumor 1 peptide greatly enhances therapeutic potential, Leukemia 29 (2015) 2238–2247.
[4] J. Liu, S. Yang, B. Cao, G. Zhou, F. Zhang, Y. Wang, R. Wang, L. Zhu, Y. Meng, C. Hu, H. Liang, X. Lin, K. Zhu, G. Chen, K.Q. Luo, L. Di, Q. Zhao, Targeting B7-H3 via chimeric antigen receptor T cells and bispecific killer cell engagers augments antitumor response of cytotoxic lymphocytes, J. Hematol. Oncol. 14 (2021) 21.
[5] L. Zhu, J. Liu, G. Zhou, T.M. Liu, Y. Dai, G. Nie, Q. Zhao, Remodeling of tumor microenvironment by tumor-targeting Nanozymes enhances immune activation of CAR T cells for combination therapy, Small 17 (2021), e2102624.
[6] B. Cao, M. Liu, L. Wang, K. Zhu, M. Cai, X. Chen, Y. Feng, S. Yang, S. Fu, C. Zhi, X. Ye, J. Zhang, Z. Zhang, X. Yang, M. Zhao, Q. Wu, L. Xu, L. Yang, H. Lian, Q. Zhao, Z. Zhang, Remodelling of tumour microenvironment by microwave ablation potentiates immunotherapy of AXL-specific CAR T cells against non-small cell lung cancer, Nat. Commun. 13 (2022) 6203.
[7] Q. Zhao, Novel chimeric antigen receptor T cells based on T-cell receptor-like antibodies, Blood Sci. 1 (2019) 144–147.
[8] J. Liu, G. Zhou, L. Zhang, Q. Zhao, Building potent chimeric antigen receptor T cells with CRISPR genome editing, Front. Immunol. 10 (2019) 456.
[9] S. Liu, V. Galat, Y. Galat, Y.K.A. Lee, D. Wainwright, J. Wu, NK cell-based cancer immunotherapy: from basic biology to clinical development, J. Hematol. Oncol. 14 (2021) 7.
[10] E. Liu, D. Marin, P. Banerjee, H.A. Macapinlac, P. Thompson, R. Basar, L. Nassif Kerbauy, B. Overman, P. Thall, M. Kaplan, V. Nandivada, I. Kaur, A. Nunez Cortes, K. Cao, M. Daher, C. Hosing, E.N. Cohen, P. Kebriaei, R. Mehta, S. Neelapu, Y. Nieto, M. Wang, W. Wierda, M. Keating, R. Champlin, E.J. Shpall, K. Rezvani, Use of CAR-transduced natural killer cells in CD19-positive lymphoid tumors, N. Engl. J. Med. 382 (2020) 545–553.
[11] G. Xie, H. Dong, Y. Liang, J.D. Ham, R. Rizwan, J. Chen, CAR-NK cells: a promising cellular immunotherapy for cancer, EBioMedicine 59 (2020) 102975.
[12] J.H. Gong, G. Maki, H.G. Klingemann, Characterization of a human cell line (NK-92) with phenotypical and functional characteristics of activated natural killer cells, Leukemia 8 (1994) 652–658.
[13] B. Cao, M. Liu, J. Huang, J. Zhou, J. Li, H. Lian, W. Huang, Y. Guo, S. Yang, L. Lin, M. Cai, C. Zhi, J. Wu, L. Liang, Y. Hu, H. Hu, J. He, B. Liang, Q. Zhao, K. Zhu, Development of mesothelin-specific CAR NK-92 cells for the treatment of gastric cancer, Int. J. Biol. Sci. 17 (2021) 3850–3861.
[14] M. Liu, W. Huang, Y. Guo, Y. Zhou, C. Zhi, J. Chen, J. Li, J. He, H. Lian, J. Zhou, X. Ye, Y. Hu, H. Hu, Z. Liu, J. Huang, L. Lin, M. Cai, X. Wang, J. Huang, Z. Zhang, K. Zhu, Q. Zhao, B. Cao, CAR NK-92 cells targeting DLL3 kill effectively small cell lung cancer cells in vitro and in vivo, J. Leukoc. Biol. 112 (2022) 901–911.
[15] S. Yang, B. Cao, G. Zhou, L. Zhu, L. Wang, L. Zhang, H.F. Kwok, Z. Zhang, Q. Zhao, Targeting B7-H3 immune checkpoint with chimeric antigen receptor-engineered natural killer cells exhibits potent cytotoxicity against non-small cell lung Cancer, Front. Pharmacol. 11 (2020) 1089.
[16] S.E. Shelton, H.T. Nguyen, D.A. Barbie, R.D. Kamm, Engineering approaches for studying immune-tumor cell interactions and immunotherapy, iScience 24 (2021) 101985.
[17] C.R. Ireson, M.S. Alavijeh, A.M. Palmer, E.R. Fowler, H.J. Jones, The role of mouse tumour models in the discovery and development of anticancer drugs, Br. J. Cancer 121 (2019) 101–108.

[18] J. Zhuo, R. Su, W. Tan, Z. Lian, D. Lu, X. Xu, The ongoing trends of patient-derived xenograft models in oncology, Cancer Commun. (Lond.) 40 (2020) 559–563.
[19] A.S. Nunes, A.S. Barros, E.C. Costa, A.F. Moreira, I.J. Correia, 3D tumor spheroids as in vitro models to mimic in vivo human solid tumors resistance to therapeutic drugs, Biotechnol. Bioeng. 116 (2019) 206–226.
[20] F. Xing, Y.C. Liu, S. Huang, X. Lyu, S.M. Su, U.I. Chan, P.C. Wu, Y. Yan, N. Ai, J. Li, M. Zhao, B.K. Rajendran, J. Liu, F. Shao, H. Sun, T.K. Choi, W. Zhu, G. Luo, S. Liu, L. Xu, K.L. Chan, Q. Zhao, K. Miao, K.Q. Luo, W. Ge, X. Xu, G. Wang, T.M. Liu, C. X. Deng, Accelerating precision anti-cancer therapy by time-lapse and label-free 3D tumor slice culture platform, Theranostics 11 (2021) 9415–9430.
[21] P. Chen, X. Zhang, R. Ding, L. Yang, X. Lyu, J. Zeng, J.H. Lei, L. Wang, J. Bi, N. Shao, D. Shu, B. Wu, J. Wu, Z. Yang, H. Wang, B. Wang, K. Xiong, Y. Lu, S. Fu, T. K. Choi, N.W. Lon, A. Zhang, D. Tang, Y. Quan, Y. Meng, K. Miao, H. Sun, M. Zhao, J. Bao, L. Zhang, X. Xu, Y. Shi, Y. Lin, C. Deng, Patient-derived organoids can guide personalized-therapies for patients with advanced breast Cancer, Adv. Sci. (Weinh) 8 (2021), e2101176.
[22] L. He, C. Deng, Recent advances in organotypic tissue slice cultures for anticancer drug development, Int. J. Biol. Sci. 18 (2022) 5885–5896.
[23] M.S. Skovgard, H.R. Hocine, J.K. Saini, M. Moroz, R.Y. Bellis, S. Banerjee, A. Morello, V. Ponomarev, J. Villena-Vargas, P.S. Adusumilli, Imaging CAR T-cell kinetics in solid tumors: translational implications, Mol. Ther. Oncolyt. 22 (2021) 355–367.
[24] E. Donnadieu, L. Dupre, L.G. Pinho, V. Cotta-de-Almeida, Surmounting the obstacles that impede effective CAR T cell trafficking to solid tumors, J. Leukoc. Biol. 108 (2020) 1067–1079.
[25] D. Chu, X. Dong, Q. Zhao, J. Gu, Z. Wang, Photosensitization priming of tumor microenvironments improves delivery of Nanotherapeutics via neutrophil infiltration, Adv. Mater. 29 (2017) 1701021.
[26] Y. Vedvyas, E. Shevlin, M. Zaman, I.M. Min, A. Amor-Coarasa, S. Park, S. Park, K. W. Kwon, T. Smith, Y. Luo, D. Kim, Y. Kim, B. Law, R. Ting, J. Babich, M.M. Jin, Longitudinal PET imaging demonstrates biphasic CAR T cell responses in survivors, JCI Insight 1 (2016), e90064.
[27] M.A. Sellmyer, S.A. Richman, K. Lohith, C. Hou, C.C. Weng, R.H. Mach, R. S. O'Connor, M.C. Milone, M.D. Farwell, Imaging CAR T cell trafficking with eDHFR as a PET reporter gene, Mol. Ther. 28 (2020) 42–51.
[28] L. Kiru, A. Zlitni, A.M. Tousley, G.N. Dalton, W. Wu, F. Lafortune, A. Liu, K. M. Cunanan, H. Nejadnik, T. Sulchek, M.E. Moseley, R.G. Majzner, H.E. Daldrup-Link, In vivo imaging of nanoparticle-labeled CAR T cells, Proc. Natl. Acad. Sci. U. S. A. 119 (2022).
[29] M.J. Miller, S.H. Wei, M.D. Cahalan, I. Parker, Autonomous T cell trafficking examined in vivo with intravital two-photon microscopy, Proc. Natl. Acad. Sci. U. S. A. 100 (2003) 2604–2609.
[30] M. Mulazzani, S.P. Frassle, I. von Mucke-Heim, S. Langer, X. Zhou, H. Ishikawa-Ankerhold, J. Leube, W. Zhang, S. Dotsch, M. Svec, M. Rudelius, M. Dreyling, M. von Bergwelt-Baildon, A. Straube, V.R. Buchholz, D.H. Busch, L. von Baumgarten, Long-term in vivo microscopy of CAR T cell dynamics during eradication of CNS lymphoma in mice, Proc. Natl. Acad. Sci. U. S. A. 116 (2019) 24275–24284.
[31] L. Zhu, J. Liu, G. Zhou, H.M. Ng, I.L. Ang, G. Ma, Y. Liu, S. Yang, F. Zhang, K. Miao, T.C.W. Poon, X. Zhang, Z. Yuan, C.X. Deng, Q. Zhao, Targeting immune checkpoint B7-H3 antibody-chlorin e6 bioconjugates for spectroscopic photoacoustic imaging and photodynamic therapy, Chem. Commun. (Camb.) 55 (2019) 14255–14258.
[32] M. Ahmed, M. Cheng, Q. Zhao, Y. Goldgur, S.M. Cheal, H.F. Guo, S.M. Larson, N. K. Cheung, Humanized affinity-matured monoclonal antibody 8H9 has potent antitumor activity and binds to FG loop of tumor antigen B7-H3, J. Biol. Chem. 290 (2015) 30018–30029.
[33] X. Tang, Y. Wang, J. Huang, Z. Zhang, F. Liu, J. Xu, G. Guo, W. Wang, A. Tong, L. Zhou, Administration of B7-H3 targeted chimeric antigen receptor-T cells induce regression of glioblastoma, Signal. Transduct. Target. Ther. 6 (2021) 125.
[34] M.V. Sheraton, G.G.Y. Chiew, V. Melnikov, E.Y. Tan, K.Q. Luo, N. Verma, P.M. A. Sloot, Emergence of spatio-temporal variations in chemotherapeutic drug efficacy: in-vitro and in-silico 3D tumour spheroid studies, BMC Cancer 20 (2020) 1201.
[35] C.-K. Chen, T.-M. Liu, Imaging morphodynamics of human blood cells in vivo with video-rate third harmonic generation microscopy, Biomed. Opt. Express 3 (2012) 2860–2865.
[36] H. Lui, Photodynamic therapy in dermatology with porfimer sodium and benzoporphyrin derivative: an update, Semin. Oncol. 21 (1994) 11–14.
[37] T. Namikawa, T. Sato, K. Hanazaki, Recent advances in near-infrared fluorescence-guided imaging surgery using indocyanine green, Surg. Today 45 (2015) 1467–1474.
[38] H. Yang, H. Jia, Q. Zhao, K.Q. Luo, Visualization of natural killer cell-mediated killing of cancer cells at single-cell resolution in live zebrafish, Biosens. Bioelectron. 216 (2022) 114616.
[39] F. Combes, E. Meyer, N.N. Sanders, Immune cells as tumor drug delivery vehicles, J. Control. Release 327 (2020) 70–87.
[40] S.G. Huang, C.I. Fong, M.Z. Xu, B.N. Han, Z. Yuan, Q. Zhao, Nano-loaded natural killer cells as carriers of indocyanine green for synergetic cancer immunotherapy and phototherapy, J. Innov. Opt. Heal Sci. 12 (2019) 1941002.
[41] F. Xu, M. Liu, X. Li, Z. Xiong, X. Cao, X. Shi, R. Guo, Loading of indocyanine green within polydopamine-coated laponite nanodisks for targeted cancer photothermal and photodynamic therapy, Nanomaterials (Basel) 8 (2018).
[42] J.R. Melamed, R.S. Edelstein, E.S. Day, Elucidating the fundamental mechanisms of cell death triggered by photothermal therapy, ACS Nano 9 (2015) 6–11.
[43] W. Chen, E.M. Goldys, W. Deng, Light-induced liposomes for cancer therapeutics, Prog. Lipid Res. 101052 (2020).
[44] T.E. Schnalzger, M.H. de Groot, C. Zhang, M.H. Mosa, B.E. Michels, J. Roder, T. Darvishi, W.S. Wels, H.F. Farin, 3D model for CAR-mediated cytotoxicity using patient-derived colorectal cancer organoids, EMBO J. 38 (2019).
[45] S.S. Lee, V.P. Bindokas, S.J. Kron, Multiplex three-dimensional mapping of macromolecular drug distribution in the tumor microenvironment, Mol. Cancer Ther. 18 (2019) 213–226.
[46] Y. Ando, E.L. Siegler, H.P. Ta, G.E. Cinay, H. Zhou, K.A. Gorrell, H. Au, B.M. Jarvis, P. Wang, K. Shen, Evaluating CAR-T cell therapy in a hypoxic 3D tumor model, Adv. Healthc. Mater. 8 (2019), e1900001.
[47] Z. Pang, Z. Wang, F. Li, C. Feng, X. Mu, Current progress of CAR-NK therapy in cancer treatment, Cancers (Basel) 14 (2022).
[48] X. Tang, L. Yang, Z. Li, A.P. Nalin, H. Dai, T. Xu, J. Yin, F. You, M. Zhu, W. Shen, G. Chen, X. Zhu, D. Wu, J. Yu, First-in-man clinical trial of CAR NK-92 cells: safety test of CD33-CAR NK-92 cells in patients with relapsed and refractory acute myeloid leukemia, Am. J. Cancer Res. 8 (2018) 1083–1089.